Morphodynamic modeling of erodible laminar channels

Olivier Devauchelle, Christophe Josserand, Pierre-Yves Lagrée, and Stéphane Zaleski
Institut Jean le Rond d'Alembert, Université Pierre et Marie Curie-Paris 6, CNRS-UMR 7190, Case 162, 4 place Jussieu, 75252 Paris Cédex 05, France

(Received 12 June 2007; published 29 November 2007)

A two-dimensional model for the erosion generated by viscous free-surface flows, based on the shallow-water equations and the lubrication approximation, is presented. It has a family of self-similar solutions for straight erodible channels, with an aspect ratio that increases in time. It is also shown, through a simplified stability analysis, that a laminar river can generate various bar instabilities very similar to those observed in natural rivers. This theoretical similarity reflects the meandering and braiding tendencies of laminar rivers indicated by F. Métivier and P. Meunier [J. Hydrol. **27**, 22 (2003)]. Finally, we propose a simple scenario for the transition between patterns observed in experimental erodible channels.

DOI: 10.1103/PhysRevE.76.056318 PACS number(s): 47.15.Rq, 47.15.Fe, 92.40.Gc, 92.40.Pb

I. INTRODUCTION

Natural rivers seldom form straight beds. Instead, they usually develop braids or meanders as a consequence of current-induced sediment transport. The understanding of such river sedimentation mechanisms can also help to characterize the spatial heterogeneity of alluvial rocks, which is a key parameter when simulating aquifer flows or oil traps in petroleum reservoirs [1]. The theoretical work in [2–4] introduced among geomorphologists the fruitful idea that such patterns may originate in the linear instability of the flow, bed, and bank system. Two-dimensional turbulent shallow water equations associated with a simple sediment transport law are able to predict the formation of alternate bars in channels of constant width. Such bars have been commonly accepted as a key phenomenon for braids and meander formation [5]. Numerous refinements of this theory may be found in the literature: [6] performed the bar stability analysis in three dimensions, while [5] focused on the differentiation between braids and meanders. Later [7,8] relaxed the rigid-banks hypothesis, and [9] and more recently [10] modeled the nonlinear evolution of free bars. All these works (and to our knowledge, every study in this field) considered turbulent flows, which is entirely legitimate as far as natural rivers are concerned (the average Reynolds number of the Seine River in Paris is about 10^6). However, one should not conclude from this ubiquity of turbulence that braiding and meandering are inherently turbulent phenomena. [11] very recently accumulated experimental evidence showing that laminar flumes may also generate many patterns created by real rivers. In particular, the constant flow of a thin liquid film down a homogeneous granular bed initially crossed by a straight channel exhibits rather complex pattern dynamics as the flume is deformed by erosion (see [12]). First, the channel widens while remaining straight. Then a meanderlike instability develops, which deforms both the bed and the banks. Eventually, more bars develop in the middle of the channel and the river starts to braid [32]. This behavior is qualitatively comparable to the one of larger channels, at higher Reynolds number (see the two meters-wide experiment in [13]). To our knowledge, no quantitative experimental results have been published about river erosion instabilities in the laminar regime. As a consequence, the results presented here can only be compared to the qualitative evolution described in [12]. Reference to turbulent experiments can only illustrate the sound similarity with the laminar case.

Our objective is to comfort the idea that microrivers can be an intermediate step toward the understanding of natural river morphodynamics. We do not claim that quantitative results from microrivers could be extrapolated to field results (see Sec. II A). We are rather convinced that such small-scale experiments share with larger ones many features still under investigation (nonlinearity of the flow-sediment interaction, equilibrium shape of the bed, behavior and influence of the bank). Such laminar flow approach can also help to disentangle the role of the turbulence in the river morphodynamics. Moreover, theoretical as well as numerical river models could be easily tested against microriver data, before adding the complexity of turbulence and switching to larger experiments and natural rivers.

In a first section, a two-dimensional evolution model for laminar flumes is presented. It is based on the assumption that the velocity profile is close to Nußelt's one. A rather general erosion law is then discussed and compared to the experiments in [14]. The following section is devoted to the study of a straight river widening process, and an analytical solution is proposed in a simple case. In the third section, the linear stability analysis of a straight laminar flume with solid banks is presented.

II. TWO-DIMENSIONAL MODEL

Let us consider an experiment during which an initial channel incised into a uniform and noncohesive sand layer is eroded by a viscous flow. If the slope of the sand bed remains small enough, one may use two-dimensional equations to model both the water flow and the sediment transport. A rather general assumption (commonly used in river mechanics) consists in the time-scale separation between the flow and erosion process: The bed evolves slowly enough for the flow to be quasistatic (see [5,4,6,8]). Of course, this hypothesis fails during such violent events as roll waves.

In the present article the following notations are used (see also Fig. 1): x and y are the coordinates in the plane of the

 ©2007 The American Physical Society

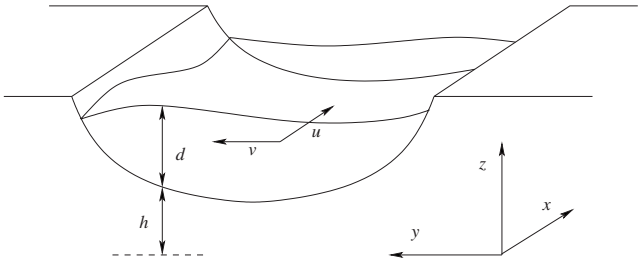

FIG. 1. Sketch of a riverbed: h is the elevation of the sand surface and d is the water depth. The axes x and z are tilted with respect to horizontal. The Saint-Venant approximation is used for the velocity field $\mathbf{u}=(u,v)$.

experiment, the first aiming toward the main slope, and z is the coordinate normal to the plate; h is the elevation of the sand surface and d is the water depth ($\eta=h+d$ is thus the water level); $\mathbf{u}=(u,v)$ is the vertically averaged water velocity, the horizontal water flux components being ud and vd; S is the plate tilt; g is the magnitude of gravity, and ν is the kinematic viscosity of water.

A. Water flow

The present microriver model requires that the water flow is laminar, so that it can be approximated by a vertical velocity profile of Nußelt type. For this assumption to hold, the Reynolds number $\mathrm{Re}=u_0 d_0/\nu$ must remain low enough (d_0 and u_0 are the typical height and velocity scales, respectively). The water velocity $\hat{\mathbf{u}}$ is thus approached by a parabolic velocity profile which adapts instantaneously to the topography:

$$\hat{\mathbf{u}}(x,y,z,t) \approx \frac{3}{2}\xi(2-\xi)(u(x,y,t),v(x,y,t),0), \tag{1}$$

where $\xi=(z-h)/d$. This method corresponds to the lubrication approximation. Different approaches may be found in [15] or [16], though in one dimension. Equation (1) allows us to define the horizontal shear stress vector $\boldsymbol{\tau}$ at the bed surface:

$$\boldsymbol{\tau} = \rho_w \nu \left.\frac{\partial \hat{\mathbf{u}}}{\partial z}\right|_{z=h} \approx 3\rho_w \nu \frac{\mathbf{u}}{d}. \tag{2}$$

Secondary currents are thus neglected, although many authors believe they strongly influence erosion in developed meanders (see, for example, [17]). The effect of secondary currents is sometimes taken into account in the shallow water framework by mean of an *ad hoc* term in sediment transport equations (see [8]). Since the present study is restricted to straight channels, we will hereafter assume that the curvature of the flow remains small enough for the secondary currents to remain negligible (this argument is developed in [18]). This approximation is actually correct for any curvature, provided the Reynolds number is low enough.

The vertical integration of the Navier-Stokes equations, associated with Eq. (1), leads to the viscous shallow water equations (sometimes named the Saint-Venant's equations):

$$\frac{6}{5}(\mathbf{u}\cdot\boldsymbol{\nabla})\mathbf{u} = g[-\boldsymbol{\nabla}(d+h)+S\mathbf{e}_x] - \frac{3\nu}{d^2}\mathbf{u}, \tag{3}$$

$$\boldsymbol{\nabla}\cdot(\mathbf{u}d) = 0, \tag{4}$$

where $\mathbf{e}_x$ is the unit vector parallel to the x axis. These equations are very similar to those used for turbulent rivers. The only differences lie in the coefficient 6/5 which becomes 1 in the turbulent case, and in the friction term $-3\nu\mathbf{u}/d^2$ which becomes $-C_f\|\mathbf{u}\|\mathbf{u}/d$ (C_f being a friction coefficient, related to the Chézy coefficient). One cannot thus expect microrivers to be scaled models for natural ones, since the laminar flow equations cannot be reduced to the classical turbulent ones. On the other hand, it is interesting to point out similarities and differences between these two different (although not too far) cases, turbulent and laminar.

B. Sediment transport

The river bed evolves under the influence of both erosion and avalanches. In the present context erosion consists of flow-induced bed-load transport of sand grains. On the other hand, avalanches are collective phenomena triggered by an excess slope of the sand surface. In the continuous model developed here, we can only handle the average effects of erosion and avalanches. This approximation allows for the definition of a total volumic sediment flux $\mathbf{q}(x,y,t)$ integrated along the vertical direction. Assuming a strong timescale separation between erosion and avalanches, one may consider the associated fluxes (respectively, $\mathbf{q}_e$ and $\mathbf{q}_a$) as independent. The continuity equation for sand then reads

$$\frac{\partial h}{\partial t} = -\boldsymbol{\nabla}\cdot\mathbf{q}, \tag{5}$$

where $\mathbf{q}=\mathbf{q}_e+\mathbf{q}_a$. Finally, closure relations have to be deduced, either on dimensional, physical, or empirical grounds in order to link Eq. (5) to the flow equations.

Erosion contribution. Most of the relations between the sediment flux and the flow are proposed in the literature as functions of the Shields number θ, which expresses the ratio between hydrodynamic forces exerted on a grain to its apparent weight:

$$\theta = \frac{\|\boldsymbol{\tau}\|}{d_s(\rho_g-\rho_w)g}, \tag{6}$$

where d_s, ρ_w, ρ_g, and $\boldsymbol{\tau}$ are, respectively, the typical particle diameter, the density of water, the density of a grain, and the bottom shear stress. As suggested in [19], we propose the following expression as a classical relationship (see the review of [20]) for small slope:

$$\mathbf{q}_e = \phi(\theta)\left(\frac{\boldsymbol{\tau}}{\|\boldsymbol{\tau}\|} - \mathbf{G}\cdot\boldsymbol{\nabla}h\right), \tag{7}$$

where ϕ is a growing function that may include a threshold value, and $\mathbf{G}$ is a diagonal operator.

To determine a plausible form for $\phi(\theta)$ we shall use recent experimental results obtained by Charru, Mouilleron, and Eiff for grain transport in the viscous flow regime [14].

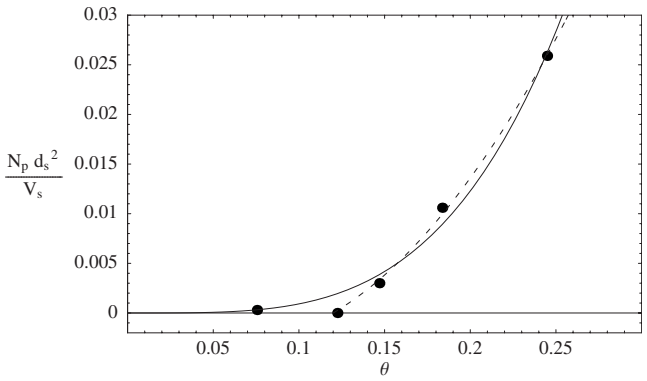

FIG. 2. Different transport laws compared with the experimental results obtained by [14]. The grains are transported by a viscous flow in a circular Hele-Shaw cell. N_p is the particle flux and V_s is the settling velocity of a particle. Dashed: Threshold law proposed by [14]; $N_p d_s/V_s = 0.85\theta(\theta-0.12)\mathcal{H}(\theta-0.12)$. Solid line: Power-law fit; $N_p d_s/V_s = 5.13\theta^{3.75}$. This law will be used as an illustrative case in the present study.

Their results on grain transports are partially reproduced in Fig. 2 and these authors suggest then the following transport law:

$$\frac{N_p d_s^2}{V_s} = 0.85\theta(\theta - 0.12)\mathcal{H}(\theta - 0.12), \tag{8}$$

where N_p is the particle flux and V_s is the Stokes settling velocity of a particle $[V_s = g d_s^2(\rho_s - \rho_w)/(18\nu\rho_w)]$. $\mathcal{H}$ is the Heaviside function. N_p is linked to q through $q = N_p\mathcal{V}$, where $\mathcal{V}$ is the volume filled by a particle in the sediment layer. According to this expression, no sediment is transported at Shields number values below a threshold. However, [14] indicates that some particles remain in motion at Shields numbers lower than 0.12 during a transition regime, and will eventually settle after an "*armoring time* $[\cdots]$ *very large compared to the hydrodynamic time scales*." Maybe due to this armoring time t_a, their measurements of the sediment flux do not exactly vanish below the threshold (see Fig. 2). According to [14], a typical dimensionless value for t_a is 10^5. In the present notations, the ratio between the erosion typical time scale T defined in Sec. III A reads

$$\frac{t_a}{T} = 10^5 \frac{\gamma\mathcal{V}}{d_s d_0^2}\left(\frac{\rho_w}{\rho_s - \rho_w} S \frac{d_0}{d_s}\right)^{\beta}, \tag{9}$$

which is typically much larger than one. The armoring phenomenon is a possible explanation for thresholds in transport laws. Since it occurs at time scales much larger than the erosion ones, it is tempting to use a pure power law function instead of formula (8), as already proposed earlier to model sediment transport under turbulent flow (such as [10] for instance). Such a law may be adjusted to fit the data of [14] (see again Fig. 2) and it gives

$$\frac{N_p d_s^2}{V_s} = 5.13\theta^{3.75}. \tag{10}$$

Relations (8) and (10) cannot be in fact clearly separated by the experiments of [14]. Thus, for simplicity reasons, we will use the second one in what follows. This choice will be discussed again in Secs. III and IV.

The above discussion suggests that the sediment transport measurements proposed in [14] should be used with great care when dealing with erosion pattern formation by laminar flows: equilibrium state may not be reached if erosion is intense enough. This question also arises in the study of real rivers, but transient sediment transport is far out the scope of the present study. The general form of the erosion law is then taken as

$$\phi(\theta) = \phi_0\theta^{\beta}, \tag{11}$$

reminding that $\phi_0 \approx 5.13\mathcal{V}V_s/d_s^2$ and $\beta \approx 3.75$ to fit the data of [14]. These values are fixed only as an illustrative case in the sequel.

The second term in Eq. (7) reproduces the slope-induced deviation of the sediment flux. [10] sets $\mathbf{G} = \gamma\mathbf{I}$ where γ is a constant of order one. This isotropic approximation is questionable, but should not influence qualitatively the results. This term is mathematically essential to cut off short wavelength instabilities (see Sec. IV B). According to the definition of the bottom shear stress (2), the sediment transport equation (7) becomes

$$\mathbf{q}_e = E_e\left(\frac{\|\mathbf{u}\|}{d}\right)^{\beta}\left(\frac{\mathbf{u}}{\|\mathbf{u}\|} - \gamma\boldsymbol{\nabla} h\right), \tag{12}$$

with $E_e = \phi_0\{3\rho_w\nu/[2gr(\rho_g - \rho_w)]\}^{\beta}$.

Avalanches. The full dynamics of avalanches is far out the scope of this study. Instead, we may propose a simple model which reproduces the following features: The sand mass is conserved through the avalanche process; there are no avalanches under a critical slope α; above the critical angle, $\mathbf{q}_a$ is directed toward the main slope and increases with the slope value.

Considering these criteria, we propose the following expression:

$$\mathbf{q}_a = -E_a\mathcal{F}(\|\nabla h\|)\frac{\nabla h}{\|\nabla h\|}, \tag{13}$$

where $\mathcal{F}(\cdot) = (\cdot - \alpha)\mathcal{H}(\cdot - \alpha)$ and E_a is a constant. Indeed, a similar law has been successfully employed for Aeolian dunes in [21].

Finally, it is important to notice here that these fluxes $\mathbf{q}_e$ and $\mathbf{q}_a$ do not account for the saltating grain dynamics. In a simplified approach, the grain motions would end up into a settling distance at which the fluxes develop (see [22] and references therein for a discussion of these terms). It manifests in the dynamics through a phase shift between the shear stress and the fluxes. By sake of simplicity, we do not take into account such a term although it could be implemented easily. Such an approximation corresponds somehow to a limit where the density ratio between grains and water is high. In the following, it is in fact remarkable that the instability exists without such a phase shift.

C. Boundary conditions

Flow equations (3) and (4) together with sediment transport equations (5), (12), and (13) form a closed system. To

solve this system in the fixed domain Ω, conditions must be specified on its boundary $\partial\Omega$. Their general form writes

$$\lambda_u d + \mu_u \mathbf{u}\cdot\mathbf{n} = \pi_u, \quad \lambda_h h + \mu_h \mathbf{q}\cdot\mathbf{n} = \pi_h, \tag{14}$$

where λ_u, μ_u, π_u, λ_h, μ_h, and π_h are functions to be specified. $\mathbf{n}$ is the 2D unit vector normal to $\partial\Omega$, aiming outward. In the general case, Ω may include subdomains where $\mathbf{q}=0$. In such domains, the evolution equation becomes $\partial h/\partial t=0$.

If one wants to restrict the analysis to the active subdomain $\Omega_+(t)$, where $\mathbf{q}\neq 0$, the conditions to be imposed on its mobile boundary $\partial\Omega_+(t)$ are

$$\mathbf{u}\cdot\mathbf{n}=0, \quad \mathbf{q}_+\cdot\mathbf{n}=c(h_+-h_-),$$

$$\frac{dh_+}{dt}+\frac{dh_-}{dt}=-\nabla\cdot\mathbf{q}_+ + c(\mathbf{n}\cdot\nabla h_+ + \mathbf{n}\cdot\nabla h_-). \tag{15}$$

In the above equations, c is the normal velocity of the frontier $\partial\Omega_+(t)$, and the subscripts $+$ and $-$ denote quantities evaluated, respectively, inside and outside $\Omega_+(t)$. d/dt is the convective derivative at a point of $\partial\Omega_+(t)$ moving with velocity $c\mathbf{n}$. The first boundary condition reflects the time-scale separation between flow and erosion (so that the condition for the normal velocity of the boundary is zero instead of c). The following ones correspond to the sediment mass conservation equations integrated over a small domain crossed by $\partial\Omega_+(t)$. A special case of Eq. (15) has been derived in [23].

The classical conditions for nonerodible and impermeable banks are obtained from Eq. (15) by setting $c=0$. In that case, and for turbulent flow, bar instabilities may develop (see [10] for stability analysis and weakly nonlinear theory of bars). The present paper shows that bar instabilities of the same nature may also develop in laminar conditions. To switch from bar to meanders and braids, the condition $c=0$ must be relaxed. In a seminal paper, [8] used an empirical estimation of c as a function of the additional stress induced by secondary flows. They also implicitly assumed that the bank material input due to erosion had no influence on the bed evolution (they set $\mathbf{q}_+\cdot\mathbf{n}=0$ despite a finite value for c). They showed that meandering results from the interaction between alternate bars instabilities and the so-called bend instability, which results from the curvature of the bank. For microrivers, their hypothesis would not hold, since beds and banks are of the same granular material. The elaboration of a bank evolution law able to model the effect of avalanches is the subject of ongoing work. The present stability analysis (Sec. IV) is restricted to channels with rigid banks ($c=0$), as were the first equivalent studies in the case of real rivers (see [4]). On the other hand, in the case of a prismatic river (Sec. III), equations are solved on the whole Ω domain, and thus no boundary conditions are required. For the full determination of the solution moreover one has to prescribe global boundary conditions on the upstream and downstream fluxes of water.

III. PRISMATIC CHANNELS

For a straight, x-invariant river, the equations derived in Sec. II turn into a one-dimensional nonlinear diffusion equation which admits self-similar solutions. The reader interested in the problem of real turbulent river cross section, a complex two-dimensional problem in the general case, may refer to [23–27] among others.

A. Nonlinear diffusion equation

For a prismatic river, any quantity only depends on time and the transverse coordinate y. The flow equations (3) and (4) thus become

$$u(y,t)=\frac{gS}{3\nu}d(y,t)^2, \quad v=0,$$

$$d(y,t)+h(y,t)=\eta(t). \tag{16}$$

The water discharge

$$Q_w=\int_{-\infty}^{\infty}(ud)dy \tag{17}$$

is usually fixed in experiments, and thus governs the evolution of $\eta(t)$. For the sake of simplicity, we will consider a different case in what follows. If η instead is fixed, this arbitrary constant may be set to zero (and thus $h=-d$). This case represents a river supplied by an infinite reservoir. The sediment transport equations (5), (12), and (13) lead to

$$\frac{\partial h*}{\partial t*}=\frac{\partial}{\partial y*}\left((-h*)^\beta\frac{\partial h*}{\partial y*}\right)-\frac{1}{\epsilon_a}\frac{\partial}{\partial y*}\left[\mathcal{F}\left(\left\|\frac{\partial h*}{\partial y*}\right\|\right)\mathrm{sgn}\left(\frac{\partial h*}{\partial y*}\right)\right]. \tag{18}$$

In the above equation, the starred quantities are dimensionless. The initial depth d_0 is the characteristic length. The typical widening time scale is defined by

$$T=\frac{d_0^2}{\gamma\phi_0}\left(\frac{d_s(\rho_g-\rho_w)}{\rho_w S d_0}\right)^\beta. \tag{19}$$

The nondimensional number $\epsilon_a=d_0^2/(TE_a)$ compares typical avalanches flux to erosion ones. It will be considered very small in what follows.

The nonlinear diffusion equation (18) may be solved numerically. A classical first-order finite-volume scheme leads to the solution presented in Fig. 3 at different times. The initial width is $w_{*,0}=2.5$, and ϵ_a is fixed to 0.1. The value of ϵ_a has a weak influence on the result, provided it is small (the same computation performed with $\epsilon_a=0.01$ gives similar results). However, the Courant, Friedrichs, and Levy condition imposes a numerical time step smaller and smaller as the value of ϵ_a is reduced. The erosion law is fixed by setting $\beta=3.75$. The influence of any other parameter of the problem, such as the Froude number or the channel slope, is embedded in the definition of the time and space scales.

Through erosion, the river widens and gets shallower, while its cross-section area remains constant. This is in qualitative accordance with experiments during which the water outflow was fixed, instead of the water level in the present theory (see [12,28,7,29]). Since the erosion law (10) presents no threshold, this widening process will never stop in the framework of this model, which may seem unreasonable.

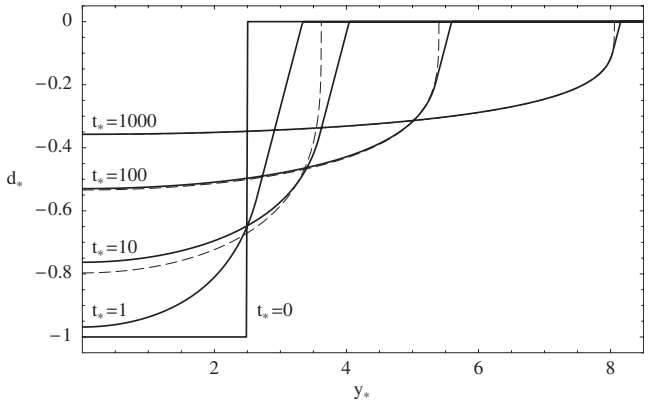

FIG. 3. Widening of a straight laminar channel through erosion, modeled with Eq. (18). Parameter values are $\epsilon_a=0.1$, $\alpha=0.8$, and $\beta=3.75$. Solid lines: Numerical solutions of Eq. (18) at different times (with avalanches). Dashed line: Self-similar solution (without avalanches, see Sec. III B) at $t*=10$, $t*=100$, and $t*=1000$. The presence of avalanches seems to influence only a small zone near the bank. The main part of the river section tends to the self-similar solution in any case.

Some authors [7,29] managed to reach an equilibrium width, but in most experiments [12,13] the channel invariance along the x axis falls before any equilibrium can be reached, due to bar instabilities ([7,29] removed the meandering tendency by using a half-river). To our knowledge, no river-widening experiments were carried out in the laminar regime at a fixed water level.

B. Self-similar solutions

If avalanches are neglected, or if the transverse slope of the channel $\partial h/\partial y$ can remain always smaller than the critical slope α (so that no avalanche occurs), the last term of Eq. (18) drops. This particular case has simple self-similar solutions of the form

$$h*(y*,t*) = \frac{1}{t*^{1/(\beta+2)}} f(\chi), \tag{20}$$

where $\chi = y*/t*^{1/(\beta+2)}$. Then Eq. (18) leads to

$$\frac{\partial}{\partial \chi}\left((-f)^{\beta}\frac{\partial f}{\partial \chi} + \frac{\chi f}{\beta+2}\right) = 0. \tag{21}$$

If f_s is a symmetrical solution to Eq. (21), $df_s/d\chi=0$ at $\chi=0$, and thus integration of Eq. (21) gives

$$f_s(\chi) = \begin{cases} -\left(\dfrac{\beta}{A-2(\beta+2)}\chi^2\right)^{1/\beta} & \text{if } \chi \in \left[0, \sqrt{A\dfrac{2(\beta+2)}{\beta}}\right], \\ 0 & \text{elsewhere,} \end{cases} \tag{22}$$

where A is a constant. Let $\mathcal{A}*$ be the (nondimensional) area of the cross section. Then

$$\mathcal{A}* = \int_0^{\infty} h*(y*,t*)dy* = -A^{1/\beta+1/2}\int_0^{\sqrt{2(\beta+2)/\beta}} \left(\frac{\beta}{2(\beta+2)}\xi^2 - 1\right)^{1/\beta} d\xi. \tag{23}$$

Thus when avalanches can be neglected, Eq. (18) admits a set of self-similar solutions parametrized by their cross-section area. The solution corresponding to $\mathcal{A}*=-2.5$ is represented on Fig. 3. Despite its rectangular initial cross section, the numerical solution converges toward its self-similar counterpart. This behavior seems quite general: It very weakly depends on the initial conditions or the value of β.

Only for $\beta=1$ (that is for an unrealistic linear erosion law) does the self-similar solution behave regularly at the banks. In that case, the river cross section is a parabola. Its width increases as $t^{1/3}$ while it shallows as $t^{-1/3}$. If the initial shape is flat enough to avoid avalanches, this condition holds at any time. Unfortunately, this case cannot model erosion pattern formation, since it is unconditionally stable (see Sec. IV).

On the other hand, if $\beta>1$ the picture is quite different. The continuous widening process still holds: the width increases as $t^{1/(\beta+2)}$, while the depth decreases as $t^{-1/(\beta+2)}$. However, in that case the bed slope $dh*/dy*$ diverges at the banks. Thus avalanches must occur at the banks, and the self-similar solution fails. This tendency is observed in laboratory experiments (see [30] among others), and was already pointed out in [23]. The effect of bank avalanches is difficult to quantify analytically. According to numerical simulations in the case $\beta=3.75$, however (see Fig. 3), they do not seem to influence strongly the bed evolution far enough from the banks. Consequently, one may still consider the results of the self-similar theory as a good approximation of the full system solutions.

IV. LINEAR STABILITY

Experimental channels such as the one of [12] or [13] often remain stable for a while, then develop meanders which in turn are followed by more complex braidedlike patterns. This scenario of transitions (sometimes called *aging*) may be interpreted as the successive dominance of different unstable modes. If the widening process presented in the previous section is slow enough, a straight river may be chosen as a quasistatic base state for a stability analysis. This is what we will assume in the following, so we will disregard any interaction between widening and instabilities.

A. Derivation of the dispersion relation

In order to present the simplest stability model which keeps the essential features of channel stability, we will consider a rectangular base state with solid-wall boundaries, of width w_0 and depth d_0 (its aspect ratio is thus $R=w_0/d_0$). The boundary conditions at the bank are $\mathbf{u}\cdot\mathbf{n}=0$ and $\mathbf{q}\cdot\mathbf{n}=0$. The basic water velocity is uniform and parallel to the x axis $[u_0=gSd_0^2/(3\nu)]$, and so is the basic sediment flux $[q_0=E_e(u_0/d_0)^{\beta}]$. Let us seek traveling-wave perturbations of this base state:

$$\varphi(x,y,t) = \varphi_0 + \epsilon\varphi_* \left(\frac{y}{w_0}\right) e^{i[kx/w_0 - \omega t/(\gamma TR)]}, \tag{24}$$

where $\varphi=(u,v,h,d,q_x,q_y)$. The base state corresponds to $\varphi_0=(u_0,0,-d_0,d_0,q_0,0)$ and the perturbation is $\varphi_*=(u_0u_*,u_0v_*,d_0h_*,d_0d_*,q_0q_{x,*},q_0q_{y,*})$. $T=d_0w_0/(\gamma Rq_0)$ is the characteristic erosion time defined in Sec. III A, and ϵ is a small dimensionless amplitude of the perturbation. k is a real dimensionless wave number whereas ω is complex in the general case. Equations (3), (4), (12), and (5), lead to the following system:

$$\left(\frac{6}{5}F^2ik + RS\right)u_* + ikh_* + (ik - 2RS)d_* = 0, \tag{25}$$

$$\left(\frac{6}{5}F^2ik + RS\right)v_* + \frac{dd_*}{dy} + \frac{dh_*}{dy} = 0, \tag{26}$$

$$ik(d_* + u_*) + \frac{dv_*}{dy} = 0, \tag{27}$$

$$-i\omega h_* + ikq_{x,*} + \frac{dq_{y,*}}{dy} = 0, \tag{28}$$

$$q_{x*} = \beta u_* - \frac{ik\gamma}{R}h_* - \beta d_*, \tag{29}$$

$$q_{y*} = v_* - \frac{\gamma}{R}\frac{dh_*}{dy}. \tag{30}$$

In the above system, $F=u_0/(gd_0)^{1/2}$ is the Froude number of the unperturbed channel. Parameters F, S, and R may be varied independently in experiments. Indeed, if Q_w is the water outflow of the river, then

$$w_0 = R\left[\left(\frac{3F\nu}{S}\right)^2\frac{1}{g}\right]^{1/3}, \tag{31}$$

$$Q_w = 3R\left(\frac{9F^8\nu^5}{gS^5}\right)^{1/3}. \tag{32}$$

The full (F,R,S) space may be explored by tuning the slope of the apparatus, the initial width of the channel, and the water outflow. Of course, the validity of the present theory requires the parameters to satisfy some conditions. First, the flow has to be laminar. The low Reynolds number condition can be easily checked:

$$\mathrm{Re} = \frac{u_0d_0}{\nu} = \frac{3F^2}{S}. \tag{33}$$

Capillarity can also cause the failure of the theory [33]. Near the banks of the channel, capillarity generates a meniscus of characteristic size l_c ($l_c=[\Gamma/(\rho g)]^{1/2}$, where Γ is the surface tension). The quantity of water flowing through the meniscus zone should remain negligible as compared to the total outflow. As a crude approximation, the outflow in the meniscus zone $Q_{w,m}$ is evaluated by Poiseuille's formula: $Q_{w,m} \sim gSl_c^4/\nu$. The condition $Q_w \gg Q_{w,m}$ thus reads

$$R \gg \left(\frac{l_c}{d_0}\right)^4. \tag{34}$$

The ratio of the water depth versus the capillary length is given by

$$\frac{d_0}{l_c} = 3^{2/3}g^{1/6}\left(\frac{\rho}{\Gamma}\right)^{1/2}\left(\frac{F\nu}{S}\right)^{2/3}. \tag{35}$$

Consequently, Eq. (34) may be satisfied for any values of R, F, and S provided the viscosity of the fluid is high enough [34]. Typical parameter values during the experiment of [12] (carried on with pure water) are $Q_w=13\times10^{-6}$ m^3 s^{-1}, $S=0.088$, and $w_0=0.1$ m. The nondimensional number of the experiment thus are $R\approx130$, $F\approx2$, $\mathrm{Re}\approx130$, and $d_0/l_c\approx0.3$. Condition (34) was not satisfied in this experiment. However, we expect that the error resulting from this failure should only affect the evaluation of nondimensional parameters from the experimental data, but the qualitative behavior predicted by the theory should hold.

If the linearized transport equations (29) and (30) are used to remove $q_{x,*}$ and $q_{y,*}$ from the mass conservation equation (28), Eqs. (25)–(28) become a system of four equations with unknowns u_*, v_*, d_*, and h_*. The velocities u_* and v_* may then be expressed as functions of d_* and h_* through the momentum equations (25) and (26). The conservation of water and sediment mass thus become a system with unknowns d_* and h_*, which in turn can be reduced to

$$\frac{d^4h_*}{dy^4} + A\frac{d^2h_*}{dy^2} + Bh_* = 0. \tag{36}$$

In the above equation,

$$\begin{aligned} A = {} & \{36F^4k^3\gamma + 30F^2k[-2k^2\gamma - ikR(1+\beta+4S\gamma) + iR\omega] \\ & + 25RS[2ik^2\gamma + kR(-3+\beta-3S\gamma) \\ & + R\omega]\}/[5(6F^2k - 5iRS)\gamma], \\ B = {} & \frac{1}{\gamma}\left\{k\left[k^3\left(\gamma - \frac{6F^2\gamma}{5}\right) + ik^2R(2\beta+3S\gamma) \right.\right. \\ & \left.\left. + \frac{1}{5}i(-5+6F^2)kR\omega + 3R^2S\omega\right]\right\}. \end{aligned} \tag{37}$$

The boundary conditions state that both the water velocity and the sediment flux vanish at the bank. Thus Eq. (30) implies that

$$\frac{dh_*}{dy}\left(\frac{1}{2}\right) = \frac{dh_*}{dy}\left(-\frac{1}{2}\right) = 0. \tag{38}$$

Equation (26) then leads to $dd_*/dy=0$ at the banks. Equation (25) implies in turn that $du_*/dy=0$ at the banks. Due to Eqs. (29) and (27), respectively, $dq_{x,*}/dy=0$ and $d^2v_*/dy^2=0$ at the banks. The sediment mass conservation (28) finally imposes that $d^2q_{y,*}/dy^2=0$ at the banks. One may then deduce from the second derivative of Eq. (30) that

$$\frac{d^3h_*}{dy^3}\left(\frac{1}{2}\right) = \frac{d^3h_*}{dy^3}\left(-\frac{1}{2}\right) = 0. \tag{39}$$

Let s_1, s_2, $-s_1$, and $-s_2$ be the four solutions of the characteristic equation attached to Eq. (36), namely

$$s^4 + As^2 + B = 0. \tag{40}$$

Then, if $C_{1,+}$, $C_{1,-}$, $C_{2,+}$, and $C_{2,-}$ are four independent constants,

$$h* = C_{1,+}e^{s_1 y} + C_{1,-}e^{-s_1 y} + C_{2,+}e^{s_2 y} + C_{2,-}e^{-s_2 y} \tag{41}$$

is a solution of Eq. (36). Such a solution must satisfy the boundary conditions (38) and (39), that is

$$\begin{aligned}
&s_1(C_{1,+}e^{s_1/2} - C_{1,-}e^{-s_1/2}) + s_2(C_{2,+}e^{s_2/2} - C_{2,-}e^{-s_2/2}) = 0,\\
&s_1(C_{1,+}e^{-s_1/2} - C_{1,-}e^{s_1/2}) + s_2(C_{2,+}e^{-s_2/2} - C_{2,-}e^{s_2/2}) = 0,\\
&s_1^3(C_{1,+}e^{s_1/2} - C_{1,-}e^{-s_1/2}) + s_2^3(C_{2,+}e^{s_2/2} - C_{2,-}e^{-s_2/2}) = 0,\\
&s_1^3(C_{1,+}e^{-s_1/2} - C_{1,-}e^{s_1/2}) + s_2^3(C_{2,+}e^{-s_2/2} - C_{2,-}e^{s_2/2}) = 0.
\end{aligned} \tag{42}$$

The determinant of the system (42) reads

$$4s_1^2 s_2^2 (s_1^2 - s_2^2)^2 \sinh(s_1)\sinh(s_2), \tag{43}$$

and vanishes only if $s = in\pi$, where n is an integer (provided s_1^2 and s_2^2 are distinct). The integer n corresponds to the number of roots of $h*$ in the width of the river. One may then derive the dispersion relation from Eq. (36):

$$\begin{aligned}
\omega = \{&5kR\{5iRS[-n^2\pi^2(-3+\beta) + 2k^2\beta]\\
&- 6F^2k[2k^2\beta + n^2\pi^2(1+\beta)]\}\\
&- i(k^2 + n^2\pi^2)(6F^2k - 5iRS)[(-5+6F^2)k^2\\
&- 5n^2\pi^2 - 15ikRS]\gamma\}/\{R(6F^2k - 5iRS)[(-5+6F^2)k^2\\
&- 5n^2\pi^2 - 15ikRS]\}.
\end{aligned} \tag{44}$$

If $A^2 = 4B$, then the roots s_1 and s_2 are equal. Similarly, if $A = 0$, s_1 is the opposite of s_2. In both cases, however, the boundary conditions impose again $s = in\pi$, and the dispersion equation (44) is still valid.

B. Results interpretation

The linear stability of a channel depends on the sign of the maximum growth rate over n and k, respectively, the transverse and longitudinal wave numbers. We will thus focus on the imaginary part σ of ω in what follows. Let σ_m be the maximum growth rate, and k_m and n_m the corresponding wave numbers [i.e., $\sigma_m = \sigma(k_m, n_m) = \max_{k\in\mathbb{R}, n\in\mathbb{N}}(\sigma)$]. The transverse wave number n characterizes the instability pattern: $n=0$ for y-invariant dunes (this mode can also initiate step-pool instability), $n=1$ for meanders, and $n>1$ for braided patterns. The present theoretical framework fails to predict the step-pool instability often observed in narrow channels [31], as σ is always negative for $n=0$. This is not surprising for the phase shift between the bed deformation and the water shear stress is neglected here (this phase shift controls sand ripple formation, see for instance [22]). For higher modes, on the other hand, a positive growth rate is possible (see Fig. 4), despite the lubrication approximation. This indicates that the instability mechanism governing bar formation is different from the phase shift induced by the advection term in the case of dunes and ripples.

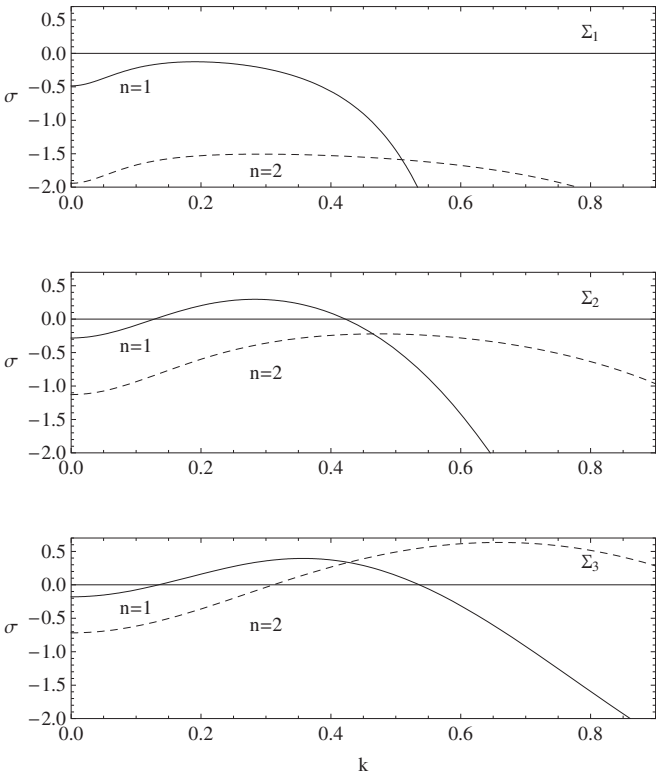

FIG. 4. Linear growth rate σ of bed instability in a laminar river, versus the corresponding nondimensional wave number k. The fixed parameter values are $\beta=3.75$, $\gamma=1$, and $S=0.0875$. The Froude number and aspect ratio are varied according to a straight river widening (see Sec. IV B and points Σ_i in Fig. 5). Above: $R_1=20.3$ and $F_1=3.94$; middle: $R_2=35.0$ and $F_2=3.21$; below: $R_3=55.0$ and $F_3=2.71$. For each set $\Sigma_i=(R_i,F_i)$, the solid curve corresponds to the mode $n=1$, whereas the dashed one corresponds to the mode $n=2$. The successive dominance of modes provides an interpretation for the transition from alternate bars to braids observed experimentally in [12].

The fluid and sediment choices determine parameters γ and β. Both parameters are crucial to the present model. The diffusion term which is proportional to γ stabilizes the high n modes. Without it, the higher n, the higher σ_m. As in [10], we take $\gamma=1$ in the following. If $\beta=1$, that is, if the sediment flux is proportional to the shear stress, then no instability ever appears (again σ is always negative in that case). Instability may occur only if $\beta>1$. $\beta=3.75$ is chosen hereinafter as an illustrative case (see Sec. II B).

Figure 4 illustrates the transition to bed instability as the aspect ratio is increased, for constant tilt and Froude number. A deep and narrow channel is stable, as for no values of n and k can σ be negative. A shift to a larger aspect ratio value allows for the $n=1$ mode to be unstable. For a still wider

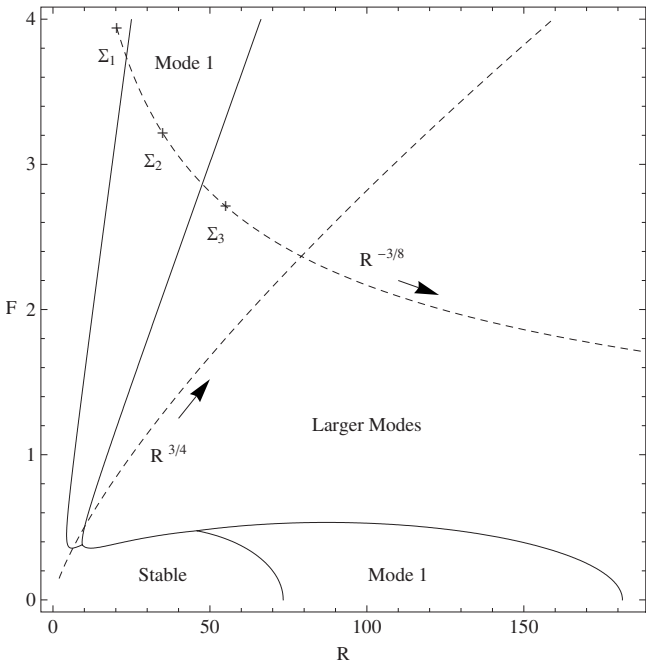

FIG. 5. Stability diagram for a laminar channel. The domains (separated by solid lines) are named after the most unstable mode between $n=1$ and $n=2$. The parameters values are $\beta=3.75$, $\gamma=1$ and $S=0.0875$. The dashed lines represent the evolution of a straight river when the water level is imposed $[F=F_0(R/R_0)^{3/4}]$ or when the outflow is imposed $[F=F_0(R/R_0)^{-3/8}]$. The three points Σ_i correspond to the three cases presented in Fig. 4.

channel, both $n=1$ and $n=2$ modes are unstable, but the latter grows faster. These transitions can be summarized in a three-dimensional phase diagram, with coordinates R, F, and S. A constant S slice of this diagram is presented in Fig. 5. The borders between domains are characterized by the following relations ($\sigma_{m,n}$ is the maximum growth rate corresponding to mode n): $\sigma_{m,1}=0$ between the stable domain and the mode 1 domain; $\sigma_{m,1}=\sigma_{m,2}$ between the mode 1 domain and the mode 2 domain; $\sigma_{m,2}=0$ between the stable domain and the mode 2 domain. Each point of the curves represented in Fig. 5 was obtained by numerical maximization of the dispersion equation.

The most surprising feature appearing on the diagram in Fig. 5 is that bars can be unstable even for vanishing Froude number (and thus for vanishing Reynolds number). In that case, inertia is completely neglected. In other words, bars may develop in a purely viscous flow, which is impossible for dunes and ripples. Since a purely viscous flow can present no transverse recirculation, the above statement proves that neither turbulence nor recirculation is inherently linked to bar formation.

The same diagram also provides a crude interpretation for the aging of laminar laboratory rivers. Let us consider for example the case of Sec. III, for which the mean water level is fixed, while its bed and banks are freely eroded. If we assume a quasistatic evolution of the bed width so that the stability analysis for fixed wall can be roughly used, we can draw a schematic scenario for the river deformation. Thus, the tilt S remains constant throughout the experiment whereas, in accordance with Eq. (22), the Froude number and aspect ratio evolve as follows:

$$R \propto t^{2/(\beta+2)}, \quad F \propto t^{3/[2(\beta+2)]}. \tag{45}$$

This parametrized curve corresponds to $F=F_0(R/R_0)^{3/4}$ in the stability diagram (the subscript 0 denotes initial conditions). In most cases this curve comes successively through the three stability domains of Fig. 5, allowing for the successive development of different bar modes. If the water output is conserved instead of the water level (this condition is more common in experiments), the straight channel evolution is characterized by

$$F = F_0(R/R_0)^{-3/8}. \tag{46}$$

Again, for realistic initial conditions ($R_0=20.3$ and $F_0=3.21$ in the experiment in [12]), the river undergoes different instability regimes as it ages. The three points Σ_i drawn on Fig. 5 would then represent three different states of the same experiment, extrapolated from the initial condition using Eq. (46). The corresponding growth rates are plotted in Fig. 4. When the highest growth rate of the first mode crosses zero, alternate bars appear, eventually replaced by higher order modes, leading to braided patterns.

If a threshold is introduced in the erosion law, the river eventually reaches an equilibrium state. The position of this equilibrium in the stability diagram is an indication about the instability patterns the river will preferentially develop. For instance, we may expect that a river will develop meanders if its equilibrium state lies in the domain where the $n=1$ mode is the most unstable one.

V. CONCLUSION

The present paper demonstrates that the equations governing the evolution of laminar microrivers are very similar to their counterparts in the turbulent case. Experimental evidence of this similarity is collected in [11]. This result suggests that microrivers could facilitate the examination of some remaining difficulties of river morphodynamics, such as nonlinearities or bank evolution. In a first attempt to develop viscous channel widening and stability theory, we presented a two-dimensional shallow-water model. A very simplified analytical approach based on this model was sufficient to describe qualitatively the aging process observed in some experiments. A diagram presenting the dominant unstable modes with respect to the channel tilt, Froude number, and aspect ratio was obtained (Fig. 5), which shows a large domain of existence for the meandering mode ($n=1$) at small (or even null) Froude number. This illustrates the sound difference between bars and dunes or ripples, which need inertia to grow.

The use of a fluid more viscous than water in experiments would allow one to reach very low Froude numbers, while reducing the perturbing effect of capillarity. The consecutive reduction of the Reynolds number would prevent recirculation, thus allowing the experimental separation between the effects of recirculation and bar instability.

The relaxation of the rigid banks hypothesis requires the development of bank erosion models, able to take avalanches into account. Such an improvement, associated with numerical simulation, would allow one to test the laminar shallow-water theory against experiments in conditions closer to natural rivers.

ACKNOWLEDGMENTS

It is our pleasure to thank B. Andreotti, P. Claudin, A. Fourrière, E. Lajeunesse, D. Lhuillier, L. Malverti, F. Métivier, and G. Parker for inspiring and stimulating discussions.

[1] G. de Marsily, F. Delay, G. J. P. Renard, V. Teles, and S. Violette, Hydrogeol. J. **13**, 161 (2005).
[2] A. Reynolds, J. Fluid Mech. **22**, 113 (1965).
[3] E. Hansen, Basic Research Report 13, Copenhagen Technical University of Denmark, 1967.
[4] R. A. Callander, J. Fluid Mech. **36**, 465 (1969).
[5] G. Parker, J. Fluid Mech. **76**, 457 (1976).
[6] F. Engelund and O. Skovgaard, J. Fluid Mech. **57**, 289 (1973).
[7] S. Ikeda, G. Parker, and K. Saway, J. Fluid Mech. **112**, 363 (1981).
[8] P. Blondeaux and G. Seminara, J. Fluid Mech. **157**, 449 (1985).
[9] M. Colombini, G. Seminara, and M. Tubino, J. Fluid Mech. **181**, 213 (1987).
[10] R. Schielen, A. Doelman, and H. de Swart, J. Fluid Mech. **252**, 325 (1993).
[11] L. Malverti, G. Parker, L. Armstrong, P. Lancien, E. Lajeunesse, F. Métivier, S. Coleman, C. E. Smith, T. Davies, and A. Cantelli, Sedimentology (to be published).
[12] F. Métivier and P. Meunier, J. Hydrol. **271**, 22 (2003).
[13] B. Federici and C. Paola, Water Resour. Res. **39**, 1162 (2003).
[14] F. Charru, H. Mouilleron, and O. Eiff, J. Fluid Mech. **519**, 55 (2004).
[15] C. Ruyer-Quil and P. Manneville, Eur. Phys. J. B **15**, 357 (2000).
[16] F. Bouchut, A. Mangeney-Castelnau, B. Perthame, and J.-P. Vilotte, C. R. Acad. Sci. Paris **336**, 531 (2003).
[17] K. Blankaert and H. de Vriend, J. Fluid Mech. **498**, 353 (2004).
[18] *River Meandering*, edited by S. Ikeda and G. Parker (AGU Water Resources Monograph, Washington, DC, 1989), Vol. 12, pp. 379–415.
[19] *Geomorphological Fluid Mechanics*, edited by N. J. Balmforth and A. Provenzale (Springer, New York, 2001), Chap. 16, pp. 394–402.
[20] *Handbook of Sediment Transport by Current and Waves*, edited by L. v. Rijn (Delft Hydraulics, Delft, The Netherlands, 1989), Vol. 12, pp. 379–415.
[21] P. Hersen, K. Andersen, H. Elbelrhiti, B. Andreotti, P. Claudin, and S. Douady, Phys. Rev. E **69**, 011304 (2004).
[22] K. K. J. Kouakou and P.-Y. Lagrée, Eur. J. Mech. B/Fluids **25**, 348 (2006).
[23] A. Kovacs and G. Parker, J. Fluid Mech. **267**, 153 (1994).
[24] G. Parker, J. Fluid Mech. **89**, 109 (1978).
[25] G. Parker, J. Fluid Mech. **89**, 127 (1978).
[26] A. Paquier and S. Khodashenas, J. Hydraul. Res. **40** (5), 603 (2002).
[27] C. Stark, Geophys. Res. Lett. **33**, L04402 (2006).
[28] L. Armstrong, Ph.D. thesis, Université Paris 7 Denis Diderot, 2003.
[29] S. Ikeda, G. Parker, and Y. Kimura, Water Resour. Res. **24**, 713 (1988).
[30] T. Nakagawa, Sedimentology **30**, 117 (1983).
[31] R. Giménez, Ph.D. thesis, Katholieke Universiteit Leuven, 2003.
[32] PE. Lajeunesse and F. Métivier (personal communication).
[33] This was observed during preliminary experiments carried out with L. Malverti and E. Lajeunesse.
[34] The idea of using highly viscous fluid in microrivers was first suggested by B. Andreotti.